Finite Frequency Noise of a Superconductor-Ferromagnet Quantum Point Contact

Audrey Cottet,[1,2] Benoit Douçot,[2] and Wolfgang Belzig[3]

[1]*Laboratoire Pierre Aigrain, Ecole Normale Supérieure, CNRS, UMR8551, 24 rue Lhomond, 75231 Paris Cedex 05, France*
[2]*Laboratoire de Physique Théorique et Hautes Énergies, Universités Paris 6 et 7, CNRS, UMR 7589, 4 place Jussieu, F-75252 Paris Cedex 05, France*
[3]*Fachbereich Physik, Universität Konstanz, D-78457 Konstanz, Germany*

(Received 6 March 2008; published 17 December 2008)

We calculate the finite-frequency current noise of a superconductor-ferromagnet quantum point contact (*SF* QPC). This signal is qualitatively affected by the spin dependence of interfacial phase shifts acquired by electrons upon reflection on the QPC. For a weakly transparent QPC, noise steps appear at frequencies or voltages determined directly by the spin dependence of interfacial phase shifts. These steps can occur at experimentally accessible temperatures and frequencies. Finite-frequency noise is thus a promising tool to characterize the scattering properties of a *SF* QPC.

DOI: 10.1103/PhysRevLett.101.257001 PACS numbers: 74.50.+r, 72.25.−b, 72.70.+m

Spin-dependent transport in mesoscopic structures with ferromagnetic elements is generating a growing interest, due to the great variety of behaviors allowed by the lifting of spin degeneracy and the possibilities of applications in the field of nanospintronics [1]. In this context, the study of finite-frequency current noise (FFCN) has raised little attention so far [2]. However, a circuit is characterized by a larger number of parameters when spin degeneracy is lifted, and current noise can thus be particularly useful to obtain more information on those parameters. Recently, superconductor-ferromagnet (*SF*) quantum points contacts (QPCs) have raised much interest as a possible source of information on the properties of *F* materials. The average current flowing through *SF* QPCs has been intensively studied (see, e.g., Ref. [3]), and the zero-frequency current noise of a single-channel *SF* QPC has been recently calculated [4]. It has been shown that these quantities are affected by the spin polarization of the QPC transmission probabilities but also by the spin dependence of interfacial phase shifts (SDIPS) acquired by electrons upon reflection on the *SF* interface. Regarding FFCN in QPCs, the normal metal–normal metal (*NN*) case has been studied theoretically [5] and experimentally [6], and the *SN* case has been addressed theoretically [7], but spin-dependent transport has not been considered so far.

In this Letter, we investigate theoretically the FFCN of a *SF* QPC. Our main result is that, for a weakly transparent contact, the FFCN is qualitatively affected by the SDIPS. More precisely, some characteristic noise steps appear at various frequencies or voltages determined directly by the SDIPS value. These steps occur at experimentally accessible temperatures and frequencies. Therefore, FFCN is a promising tool to characterize the scattering properties of a *SF* QPC. More generally, this work illustrates that FFCN can provide an interesting insight in spin-dependent transport.

We define the nonsymmetrized current noise $S(V,\omega)=\int_{-\infty}^{+\infty}\langle\Delta\hat{I}(0)\Delta\hat{I}(t)\rangle e^{i\omega t}dt$ of a *SF* contact, with $\Delta\hat{I}(t)=\hat{I}(t)-\langle I\rangle$ and $\hat{I}$ the current operator of the contact. In general, $S(V,\omega)\neq S(V,-\omega)$, because $S(V,\omega)$ describes photon emission (absorption) processes between the system and a detector for $\omega>0$ ($\omega<0$). The excess noise $S_{\rm ex}(\omega)=S(V,\omega)-S(V=0,\omega)$ is often the relevant observable in experiments [6,8–12]. Interestingly, $S_{\rm ex}$ has already been measured for both signs of ω [12]. We first consider a general ballistic *SF* contact, with *S* a conventional superconductor described by the Bogoliubov–de Gennes (BdG) equations [13]. A bias voltage *V* is applied to the contact, so that the Fermi level of *S* [*F*] can be set to $\mu_S=0$ [$\mu_F=-eV$]. We denote with $\sigma\in\{\uparrow,\downarrow\}$ an electronic spin component collinear to the polarization of *F*. Electron states in the σ-spin band [denoted (e,σ)] at an energy ε and hole states in the $-\sigma$ spin band [denoted $(h,-\sigma)$] at an energy $-\varepsilon$ are coupled coherently by Andreev reflections occurring at the *SF* interface. Using the scattering approach [5], we find

$$S(V,\omega)=\frac{e^2}{h}\sum_{\substack{M,P,\\ \gamma,\eta,\alpha,\beta}}\lambda(\alpha)\lambda(\beta)\int_{-\infty}^{+\infty}d\varepsilon P_{M,P}^{\gamma,\eta}(\varepsilon,\varepsilon+\omega)\times\mathrm{Tr}[\mathcal{A}_{F,M,P}^{\alpha,\gamma,\eta}(\varepsilon,\varepsilon+\hbar\omega)\mathcal{A}_{F,P,M}^{\beta,\eta,\gamma}(\varepsilon+\hbar\omega,\varepsilon)]. \quad (1)$$

Here capital Latin indices correspond to the lead *F* or *S*, and Greek indices correspond to the electron or hole band of the space $\mathcal{E}_\sigma=\{(e,\sigma),(h,-\sigma)\}$. We use $\mathcal{A}_{F,M,P}^{\gamma,\alpha,\eta}(\varepsilon,\varepsilon')=\mathbb{I}_{F,\gamma}\delta_{F,M}\delta_{F,P}\delta_{\gamma,\alpha}\delta_{\gamma,\eta}-[\mathcal{S}_{F,M}^{\gamma,\alpha}(\varepsilon)]^\dagger\mathcal{S}_{F,P}^{\gamma,\eta}(\varepsilon')$, where $\mathcal{S}_{F,M}^{\gamma,\alpha}(\varepsilon)$ is the scattering matrix accounting for the transmission of quasiparticles with energy ε from a state of type α in lead *M* to a state of type γ in lead *F*. We define $\lambda[(e,\sigma)]=-1$, $\lambda[(h,-\sigma)]=+1$, and $P_{M,P}^{\gamma,\eta}(\varepsilon,\varepsilon')=[1-f_M^\gamma(\varepsilon)]f_P^\eta(\varepsilon')$, with $f_M^\gamma(\varepsilon)=\{1+\exp[(\varepsilon+\lambda[\gamma]\mu_M)/k_BT]\}^{-1}$ and *T* the temperature. We denote by $e=|e|$ the absolute value of the electron charge and $\mathbb{I}_{F,\gamma}$ the identity matrix in the subspace of states of type γ of

lead F. In the limit $T = 0$, using the symmetry of the BdG equations (see Ref. [4], Appendix A) and the unitarity of $\mathcal{S}(\varepsilon)$, one finds

$$S_{\rm ex}(\omega) = S_d(\omega) + \frac{e^2}{h}\Big(\int_{-\hbar|\omega|}^{0} d\varepsilon {\rm Tr}[\tilde{F}_1(\varepsilon,\omega,V)] + \int_{-e|V|}^{-\hbar|\omega|} d\varepsilon {\rm Tr}[\tilde{F}_2(\varepsilon,\omega,V)]\Big) \quad (2)$$

for $0 < |\hbar\omega| < e|V|$,

$$S_{\rm ex}(\omega) = S_d(\omega) + \frac{e^2}{h}\int_{-e|V|}^{e|V|-\hbar|\omega|} d\varepsilon {\rm Tr}[\tilde{F}_1(\varepsilon,\omega,V)] \quad (3)$$

for $eV < |\hbar\omega| < 2e|V|$, and $S_{\rm ex}(\omega) = S_d(\omega)$ for $|\hbar\omega| > 2e|V|$, with

$$S_d(\omega) = \frac{2e^2}{h}\theta(-\omega)\int_{-e|V|}^{0} d\varepsilon {\rm Re}[{\rm Tr}[\tilde{F}_3(\varepsilon,\omega,V)]] \quad (4)$$

and $\theta(\omega) = [1 + {\rm sgn}(\omega)]/2$. We define, for $i \in \{1,2,3\}$, $\tilde{F}_i(\varepsilon,\omega,V) = \sum_\sigma F_{i,\sigma}^{{\rm sgn}[V]\varepsilon,{\rm sgn}[V]|\omega|}$, with

$$F_{1,\sigma}^{\varepsilon,\omega} = s_{ee}^{\sigma}(\varepsilon)s_{ee}^{\sigma\dagger}(\varepsilon)s_{eh}^{\sigma}(\varepsilon+\hbar\omega)s_{eh}^{\sigma\dagger}(\varepsilon+\hbar\omega) - {\rm Re}[s_{ee}^{\sigma}(\varepsilon)s_{he}^{\sigma\dagger}(\varepsilon)s_{hh}^{\sigma}(\varepsilon+\hbar\omega)s_{eh}^{\sigma\dagger}(\varepsilon+\hbar\omega)], \quad (5)$$

$$F_{2,\sigma}^{\varepsilon,\omega} = 2{\rm Re}[s_{ee}^{\sigma\dagger}(\varepsilon)s_{ee}^{\sigma}(\varepsilon+\hbar\omega)s_{he}^{\sigma\dagger}(\varepsilon+\hbar\omega)s_{he}^{\sigma}(\varepsilon)] + \sum_{a\in\{e,h\}} s_{ae}^{\sigma}(\varepsilon)s_{ae}^{\sigma\dagger}(\varepsilon)[\mathbb{I}_\sigma - s_{ae}^{\sigma}(\varepsilon+\hbar\omega)s_{ae}^{\sigma\dagger}(\varepsilon+\hbar\omega)], \quad (6)$$

and

$$F_{3,\sigma}^{\varepsilon,\omega} = \sum_{a\in\{e,h\}} \lambda_a s_{ae}^{\sigma\dagger}(\varepsilon)[s_{ae}^{\sigma}(\varepsilon-\hbar\omega) - s_{ae}^{\sigma}(\varepsilon+\hbar\omega)]. \quad (7)$$

We have used above $s_{ab}^{\sigma}(\varepsilon) = S_{F,F}^{p(a,\sigma),p(b,\sigma)}(\varepsilon)$, with $p(e[h],\sigma) = (e[h],\pm\sigma)$, $\lambda_{e[h]} = \mp 1$, and $\mathbb{I}_\sigma = \mathbb{I}_{F,(e,\sigma)}$. At last, S can be obtained from $S_{\rm ex}$ using

$$\frac{S(V=0,\omega)h}{2e^2} = \theta(-\omega)\sum_\sigma \int_0^{-\hbar\omega} d\varepsilon {\rm Re}[{\rm Tr}[K_\sigma^\omega(\varepsilon)]], \quad (8)$$

with $K_\omega^\sigma(\varepsilon) = \mathbb{I}_\sigma - \sum_a \lambda_a s_{ae}^{\sigma\dagger}(\varepsilon)s_{ae}^{\sigma}(\varepsilon+\hbar\omega)$.

In the following, we consider a single-channel SF QPC, which can be modeled as a clean SN contact in series with a NF contact, with the length of N tending to zero [14]. The scattering matrix $\mathcal{P}^\sigma$ of the NF contact can be expressed as $\mathcal{P}_{FF(NN)}^{\sigma} = r_\sigma \exp[i\varphi_{FF(NN)}^{\sigma}]$ and $\mathcal{P}_{NF(FN)}^{\sigma} = t_\sigma \exp[i\varphi_{NF(FN)}^{\sigma}]$, with $r_\sigma^2 + t_\sigma^2 = 1$ and $\varphi_{NN}^{\sigma} + \varphi_{FF}^{\sigma} = \varphi_{NF}^{\sigma} + \varphi_{FN}^{\sigma} + \pi[2\pi]$. In general, the scattering phases φ_{ij}^{σ}, with $(i,j) \in \{N,F\}^2$, are spin-dependent because the QPC displays a spin-dependent scattering potential. This so-called SDIPS modifies qualitatively the behavior of the QPC. A step approximation for the gap Δ of S leads to an SN Andreev reflection amplitude $\gamma = (\varepsilon - i\sqrt{\Delta^2 - \varepsilon^2})/\Delta$ for $|\varepsilon| < \Delta$ and $\gamma = [\varepsilon - {\rm sgn}(\varepsilon)\sqrt{\varepsilon^2 - \Delta^2}]/\Delta$ for $|\varepsilon| > \Delta$ [15]. The resulting scattering matrix $\mathcal{S}(\varepsilon)$ can be found in Ref. [4], Appendix B. Importantly, the elements of $\mathcal{S}(\varepsilon)$ involve the denominator $D_\sigma(\varepsilon) = 1 - \gamma^2 r_\sigma r_{-\sigma} \times e^{i(\varphi_{NN}^{\sigma} - \varphi_{NN}^{-\sigma})}$, which accounts for iterative reflection processes between the SN and NF interfaces (Andreev bound states). A quasiparticle can interfere with itself after two back and forth travels between S and F, one as an electron (e,σ) and one as a hole $(h,-\sigma)$, which leads to a dependence of D_σ on the SDIPS parameter $\Delta\varphi = \varphi_{NN}^{\uparrow} - \varphi_{NN}^{\downarrow}$. We have checked analytically that $S(V,\omega)$ depends on the phases of $\mathcal{P}^\sigma$ through $\Delta\varphi$ only, for all values of ω, V, and T. For simplicity, we will consider below that t_σ and $\Delta\varphi$ are independent of ε and V, so that the energy dependence of $\mathcal{S}(\varepsilon)$ stems only from γ. We will mainly focus on the regime of weak transparency $T_{av} = (t_\uparrow^2 + t_\downarrow^2)/2 \ll 1$, with a finite polarization $P = (t_\uparrow^2 - t_\downarrow^2)/(t_\uparrow^2 + t_\downarrow^2)$. We will use $T = 0$ except in Fig. 3, right panel.

We now study the frequency parity of $S_{\rm ex}$. For $0 < e|V|$, $|\hbar\omega| \ll \Delta$, the function $S_d(\omega)$ can be neglected from Eqs. (2) and (3), so that one finds $S_{\rm ex}(\omega) = s_0(|V| - \hbar|\omega/2e|)\theta(2e|V| - \hbar|\omega|)$, with $s_0 = 4(e^3/h)\sum_\sigma {\rm Tr}\{s_{he}^{\sigma\dagger}(0)s_{he}^{\sigma}(0)[1 - s_{he}^{\sigma\dagger}(0)s_{he}^{\sigma}(0)]\}$ the zero-frequency differential noise. In this regime, $S_{\rm ex}$ is thus an even function of ω, determined by zero-frequency properties only. The behavior of $S_{\rm ex}$ is much richer for $eV > \Delta$. Figure 1 shows $S_{\rm ex}$ versus ω, for $eV = 1.4\Delta$ and different values of $\Delta\varphi$. We find that $S_{\rm ex}$ is not an even function of ω anymore, because Andreev reflections make $\mathcal{S}(\varepsilon)$ strongly energy-dependent [see Eq. (7)] [16]. Hence, it can be useful to measure $S_{\rm ex}$ for both signs of ω, to gain additional information on the QPC. Interestingly, $S_{\rm ex}(\omega) \neq S_{\rm ex}(-\omega)$

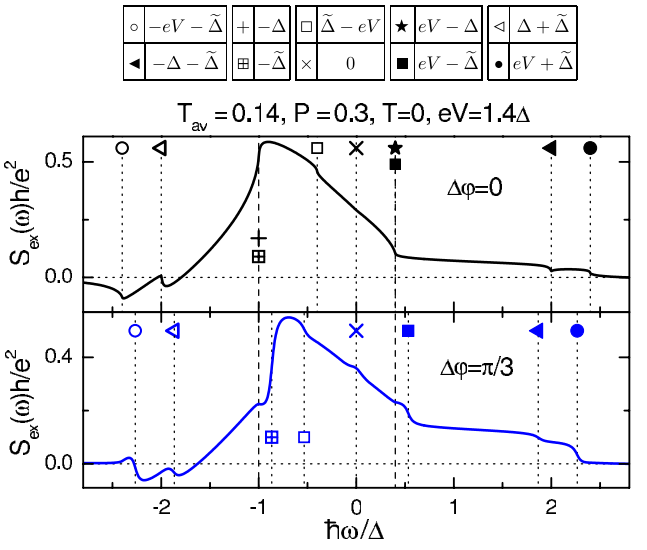

FIG. 1 (color online). Excess noise $S_{\rm ex}$ versus ω, for $V = 1.4\Delta$, $T = 0$, and different values of the SDIPS parameter $\Delta\varphi$. The symbols correspond to frequencies defined in the above table.

has already been observed in a Josephson junction [12]. We now focus on the sign of S_{ex}. For $\omega > 0$ and $T = 0$, one always finds $S_{ex} \geq 0$, because emission processes are forbidden for $V = 0$ [see Eq. (8)], so that $S_{ex} = S$ at positive frequencies. However, nothing forbids to have $S_{ex} < 0$ for $\omega < 0$, as illustrated by Fig. 1. Note that $S_{ex} < 0$ has already been predicted for a noninteracting conductor with energy-dependent transmission probabilities [17] and an interacting quantum wire [18]. However, in experimental works such a behavior has not been reported yet.

We now study the frequency dependence of S_{ex}. For $\Delta\varphi = 0$ (top panel of Fig. 1), S_{ex} shows various singularities, which can be understood from Eq. (1). The current noise at frequency ω involves a coupling between quasiparticle states with energy $\varepsilon_1 = \varepsilon$ and $\varepsilon_2 = \varepsilon + \hbar\omega$. The occupation of states in F is discontinuous at $\varepsilon = \pm eV$, and the density of states in S is singular at $\varepsilon = \pm\Delta$. This allows singularities of S_{ex} at frequencies $\omega = (\varepsilon_1 - \varepsilon_2)/\hbar$, with $(\varepsilon_1, \varepsilon_2) \in \{eV, -eV, \Delta, -\Delta\}^2$, i.e., $\hbar|\omega| \in \{0, |\Delta \pm eV|, 2\Delta, 2e|V|\}$, as already found by Ref. [7] for a SN QPC with $\omega > 0$ [19]. These different frequencies can be represented on the energy diagram of the circuit [see Fig. 2(a) for the case $eV > \Delta$]. In Fig. 1, we find that S_{ex} displays an extra noise singularity at $\hbar\omega = -\Delta$, because it involves $S(V = 0, \omega)$. For $\Delta\varphi \neq 0$, the denominator $D_\sigma(\varepsilon)$ is resonant at subgap energies $\varepsilon = \sigma\tilde{\Delta}$, with $\tilde{\Delta} = \Delta\cos(\Delta\varphi/2)$. This reveals that subgap resonances occur in the N layer [4]. This effect modifies qualitatively the behavior of the QPC: In Fig. 1, bottom panel, noise steps appear at $\hbar|\omega| \in \{|\tilde{\Delta} \pm eV|, \Delta + \tilde{\Delta}\}$ and $\hbar\omega = -\tilde{\Delta}$, marked with the symbols ○, ◁, ⊞, □, ■, ◀, and ●. These steps are due to particle transfer processes which involve the subgap resonance in the N layer. For instance, the step occurring at $\omega = eV - \tilde{\Delta}$, marked with ■ in Fig. 1, corresponds, e.g., to the Andreev reflection of electrons with energy eV of lead F, via the Andreev subgap resonance at energy $\tilde{\Delta}$ [see Fig. 2(b), blue arrow]. Importantly, for $\Delta\varphi = 0$, the SDIPS-induced noise steps are absorbed into the noise singularities of the $\Delta\varphi = 0$ case which are thus reinforced, because $|D_\sigma(\varepsilon)|^2$ is resonant at $\varepsilon = \pm\Delta$. When $\Delta\varphi \neq 0$, the singularities which existed for $\Delta\varphi = 0$ are either smoothed, like the singularity at $\hbar\omega = eV - \Delta$ (marked with ★) and the singularity at $\hbar\omega = -\Delta$ (marked with +), or even vanish. Measuring the frequencies of the steps appearing in S_{ex} can give a direct access to the SDIPS parameter $\Delta\varphi$, since these frequencies are merely linear combinations of $\tilde{\Delta}$, V, and Δ, independently of any other parameter. Moreover, V does not affect the positions of all of the singularities and steps of S_{ex} in the same manner (see the table in Fig. 1), which can help to identify these features in an experiment. In practice, the frequency range studied in Fig. 1 should be accessible with on-chip detectors, which presently allow one to reach $\omega \sim$ 250 GHz [11,20].

The left and right panels of Fig. 3 show how S_{ex} depends on the spin-averaged transmission probability T_{av} of the

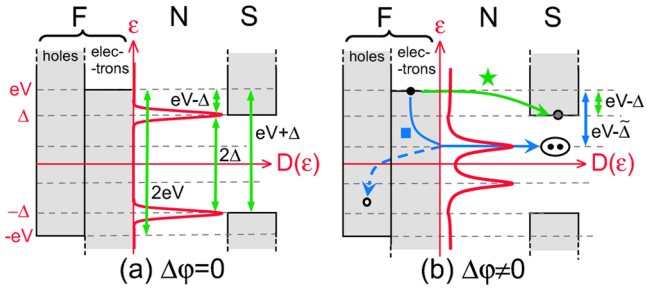

FIG. 2 (color online). Energy diagram of the SF QPC, for $\Delta\varphi \neq 0$, $eV > \Delta$, $\Delta\varphi = 0$ (a), and $\Delta\varphi \neq 0$ (b). The various columns represent the (hole) electron band in F, filled (down) up to the energy $(-)eV$, and the density of states in S, which presents a gap for $\varepsilon \in [-\Delta, \Delta]$. The resonance function $D(\varepsilon) = |D_\uparrow(\varepsilon)|^{-2} + |D_\downarrow(\varepsilon)|^{-2}$ is shown with red full lines. In (a), the different frequencies ω at which S_{ex} is singular are represented with green arrows. In (b), we show with blue and green arrows transfer processes contributing to the ★ and ■ features of Fig. 1.

QPC and on the temperature T, respectively. For brevity, we present results for $\omega > 0$ only. The singularities and steps displayed by S_{ex} remain visible for experimentally accessible temperatures (see right panel, blue curve, for $k_B T = 0.05\Delta$). Remarkably, T and T_{av} do not influence the visibility of all of the steps and singularities of S_{ex} in the same way. Those occurring for $\hbar\omega \in \{eV - \Delta, eV \mp \tilde{\Delta}\}$, marked with ★, ■, and ●, are very sharp when T_{av} and T are small (see left panel, red curve). The visibility of these features decrease when T_{av} or T increase, due to a smoothing of $|D_\sigma(\varepsilon)|^2$ or of the Fermi factors, respectively. The step occurring at $\hbar\omega = \Delta + \tilde{\Delta}$, marked with ◀, has a significantly different behavior. First, it is smoothed by an increase in T but much more slowly than the other singularities. This is due to the fact that the dependence of S on Δ and $\tilde{\Delta}$ occurs through the scattering matrix of the QPC, which does not depend on T, whereas V occurs through the Fermi factors. Second, this step vanishes for T_{av} large but also for T_{av} small. From a detailed analysis of Eq. (5), this last behavior can be traced to the fact that

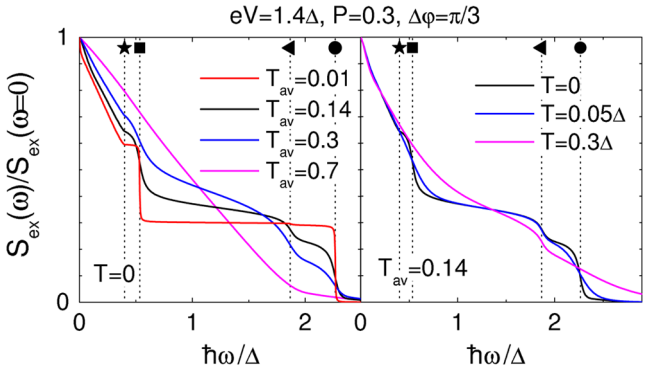

FIG. 3 (color online). Excess noise S_{ex} versus ω. The left and right panels show the effect of an increase of the spin-averaged transmission probability T_{av} and of the temperature T, respectively. The symbols correspond to frequencies defined in Fig. 1.

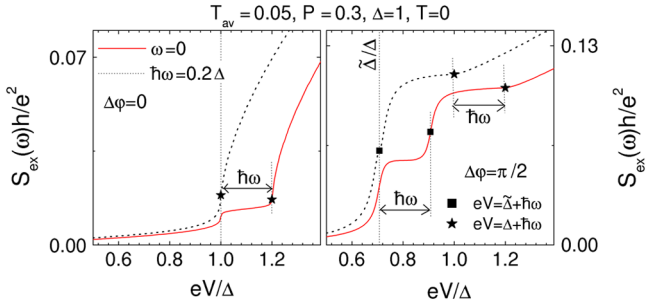

FIG. 4 (color online). Excess noise S_{ex} as a function of the bias voltage V, for $\omega = 0$ [$\omega \neq 0$] (dotted [full] lines). We have used no SDIPS on the left panel and a finite SDIPS on the right panel.

$s^{\sigma}_{ee}(\varepsilon)$ is almost constant around $\varepsilon = \Delta$ at low transparencies.

Finally, we study the dependence of S_{ex} on the bias voltage V, which can be measured, e.g., using cryogenic low noise amplifiers [6]. The left and right panels of Fig. 4 show curves calculated for a weakly transparent contact, without and with a SDIPS, respectively. For simplicity, we focus on the range $eV < 2\Delta$. For $\Delta\varphi = 0$ and $\omega = 0$, S_{ex} presents a single singularity at $V = \Delta/e$. This singularity follows straightforwardly from Eq. (1), but it has not appeared in Fig. 1 because its position is independent of ω. For $\Delta\varphi = 0$ and $\omega \neq 0$, a second singularity appears, at $V = (\Delta + \hbar\omega)/e$. This feature corresponds to the step at $\hbar\omega = eV - \Delta$ in Fig. 1. When $\Delta\varphi \neq 0$, a single singularity occurs, at $V = (\Delta + \hbar\omega)/e$. It is softer than in the case $\Delta\varphi = 0$, similarly to what happens for the singularity at $\hbar\omega = eV - \Delta$ in Fig. 1. Furthermore, two noise steps appear at $V = \tilde{\Delta}/e$ and $V = (\tilde{\Delta} + \hbar\omega)/e$. Although cryogenic low noise amplifiers are presently limited to 8 GHz [6], they should allow one to observe the features described in this paragraph since they can occur at frequencies much lower than Δ [20]. The SDIPS already modifies qualitatively the noise curve for $\omega = 0$, but we think that a measurement at $\omega \neq 0$ will be crucial in practice. It will allow one to confirm the nature of the singularities and steps occurring in S_{ex}, and it will also help to calibrate the observed $\tilde{\Delta}$ and Δ, thanks to the scale $\hbar\omega$ which appears naturally in the noise curves (see Fig. 4, horizontal arrows).

So far, experiments on SF point contacts have been performed in the limit of a large number of channels. However, we believe that the few channels regime may be realized, using, e.g., a scanning tunneling microscope (STM). Indeed, STMs allow one to reach the few channels regime (atomic contact) [21], and they are particularly suitable for making hybrid contacts. Moreover, current noise has already been measured in a STM [22]. Another possibility could be to contact a carbon nanotube to a F [23] and a S [24]. Interestingly, a multichannel ballistic SF contact has been considered in Ref. [25], using a rectangular potential barrier model. Although the transverse momentum of particles has been taken into account, the SDIPS is found to be approximately independent of the channel index when F is strongly polarized [4]. We think that the SDIPS-induced noise steps are bound to persist in these conditions. More generally, in the multichannel case, the occurrence of the SDIPS-induced noise steps will depend on the detailed structure of the contact.

In summary, we have calculated the finite-frequency nonsymmetrized current noise of a SF QPC. For low transparencies, this quantity is qualitatively modified by the spin dependence of interfacial phase shifts, which induces characteristic noise steps at various frequencies and voltages. Finite-frequency noise can thus be an interesting tool to characterize the scattering properties of a SF QPC.

We acknowledge financial support by the Swiss National Science Foundation, the German Research Foundation (DFG) through SFB 767, and the Landesstiftung Baden-Württemberg. We thank C. Glattli and T. Kontos for discussions.

[1] G. Prinz, Science **282**, 1660 (1998).
[2] A. Cottet, W. Belzig, and C. Bruder, Phys. Rev. B **70**, 115315 (2004); M. Braun, J. König, and J. Martinek, *ibid.* **74**, 075328 (2006).
[3] R. J. Soulen *et al.*, Science **282**, 85 (1998).
[4] A. Cottet and W. Belzig, Phys. Rev. B **77**, 064517 (2008).
[5] Ya. M. Blanter and M. Büttiker, Phys. Rep. **336**, 1 (2000).
[6] E. Zakka-Bajjani *et al.*, Phys. Rev. Lett. **99**, 236803 (2007).
[7] J. Torrès, T. Martin, and G. B. Lesovik, Phys. Rev. B **63**, 134517 (2001).
[8] R. J. Schoelkopf *et al.*, Phys. Rev. Lett. **78**, 3370 (1997); R. Aguado and L. P. Kouwenhoven, *ibid.* **84**, 1986 (2000).
[9] R. Deblock *et al.*, Science **301**, 203 (2003).
[10] T. K. T. Nguyen *et al.*, Phys. Rev. B **76**, 035421 (2007).
[11] E. Onac *et al.*, Phys. Rev. Lett. **96**, 176601 (2006).
[12] P.-M. Billangeon *et al.*, Phys. Rev. Lett. **96**, 136804 (2006).
[13] P. G. de Gennes, *Superconductivity of Metals and Alloys* (Benjamin, New York, 1966).
[14] C. W. J. Beenakker, Phys. Rev. B **46**, 12 841 (1992).
[15] G. E. Blonder, M. Tinkham, and T. M. Klapwijk, Phys. Rev. B **25**, 4515 (1982).
[16] For *NN* QPCs, $S_{ex}(\omega) = S_{ex}(-\omega)$ is often found (see, e.g., Refs. [9,10]), due to the hypothesis of energy-independent scattering [see Eq. (7)].
[17] G. B. Lesovik and R. Loosen, Z. Phys. B **91**, 531 (1993).
[18] F. Dolcini *et al.*, Phys. Rev. B **75**, 045332 (2007).
[19] The singularity at $\hbar\omega = 2$ eV always occurs because it is due to the cancellation of S_{ex} at ω large. However, this feature is outside the range of Fig. 1.
[20] If S is, e.g., an Al electrode, one has $\Delta \sim 46$ GHz.
[21] J. G. Rodrigo *et al.*, J. Phys. Condens. Matter **16**, R1151 (2004).
[22] H. Birk, M. J. M. de Jong, and C. Schönenberger, Phys. Rev. Lett. **75**, 1610 (1995).
[23] A. Cottet *et al.*, Semicond. Sci. Technol. **21**, S78 (2006).
[24] A. Yu. Kasumov, Science **284**, 1508 (1999).
[25] B. P. Vodopyanov, JETP Lett. **87**, 328 (2008).